







Spin-Polarized Photoelectrons in the Vicinity of Spectral Features

Stefanos Carlström ^{1,2,*} Rezvan Tahouri ² Asimina Papoulia ² Jan Marcus Dahlström ²
Misha Yu Ivanov ^{1,3,4} Olga Smirnova ^{1,5,4} and Serguei Patchkovskii¹

¹Max-Born-Institut, Max-Born-Straße 2A, 12489 Berlin, Germany

²Department of Physics, Lund University, Box 118, SE-221 00 Lund, Sweden

³Institut für Physik, Humboldt-Universität zu Berlin, Newtonstraße 15, 12487 Berlin, Germany

⁴Technion, Israel Institute of Technology, 3200003 Haifa, Israel

⁵Technische Universität Berlin, Ernst-Ruska-Gebäude, Hardenbergstraße 36A, 10623 Berlin, Germany

(Dated: November 26, 2024)

It has been shown by Fano [1] that photoionization of a caesium atom by a laser pulse tuned to the vicinity of a Cooper minimum generates spin-polarized electrons. Here we show that while photoionization of rare gases does not provide large spin polarization in the vicinity of the Cooper minimum, the Fano resonances yield much higher overall spin polarization ($\geq 40\%$). The spin polarization increases in angle-resolved photoelectron spectra, and reaches 100% when measured in coincidence with the photoion. We provide a general framework for achieving spin polarization in photoionization irrespective of the ionization regime.

Keywords: Spin polarization, Fano resonances, Cooper minima, giant resonances

The efficient generation of spin-polarized electrons is interesting for a multitude of reasons, including the table-top, laser-driven particle accelerators [2, 3], and more recently, a proposed Bell test of quantum entanglement [4]. To generate spin-polarized photoelectrons from multi-electron atoms, several prerequisites have to be satisfied [5]. First, spin-orbit interaction is needed to entangle spin and angular degrees of freedom. Whenever the photoionization amplitudes exhibit sensitivity to orbital angular momentum, we may thus expect selectivity with respect to spin. Second, a mechanism is needed to break the balance in ionization to continua with different combinations of spin S and orbital L angular momenta. As the ionizing laser field couples to the orbital angular momentum rather than spin, selectivity in ionization with respect to different orbital angular momenta is also needed.

These general principles are already implicit in the pioneering work of Fano [1]. He suggested to generate spin-polarized photoelectrons by taking advantage of the Cooper minimum (CM) found in photoionization of caesium. Starting from a $6s\ ^1S_0$ ground state, σ^+ circularly polarized light will generate p_+ photoelectrons. For spin-up electrons, this will predominantly lead to the $J = 3/2$ ionization channel, and to the $J = 1/2$ ionization channel for spin-down electrons. In these channels, the Cooper minima appear slightly shifted energetically with respect to each other, allowing us to select the desired ionization channel, and thus dominant spin contribution, by tuning the photon energy. From the conservation of angular momentum perspective, the spin-orbit coupling transfers spin-angular momentum of the photon to the emitted electron. This prediction was experimentally confirmed by Heinzmann *et al.* [6], with a spin polarization $\geq 80\%$.

In the case of few-photon ionization, using intermediate resonances with bound states may allow one to enhance a desired J -dependent ionization pathway to achieve high spin polarization [7]. In the strong field ionization regime known as nonadiabatic optical tunneling [8], electron tunneling through the barrier created by circularly polarized field and the core po-

tential is also selective with respect to the angular momentum of the tunneling electron, leading to spin polarization predicted in [2, 5, 9, 10] and experimentally confirmed in [11, 12]. The required selectivity in ionization to continua with different J arises from the exponential sensitivity of the tunneling process to the J -dependent ionization potential.

Here we return to the one-photon regime originally studied by Fano, but focus on the role of the continuum resonances bearing his name. We use *ab initio* calculations to describe photoionization of argon and xenon in a broad energy range of photon energies (up to 250 eV). This includes the autoionizing resonances leading up to the ns , $J = 1/2$ (argon and xenon), and $4d$, $J = 3/2$ and $J = 5/2$ (xenon) thresholds (double ionization, which would broaden some Fano lines [13], is not included).

In view of the general scheme outlined above, these resonances offer important advantages. First, they exhibit a strong angular dependence. Second, their minima are clear and sharp, in contrast to shallow spectral features such as the CM or shape resonances. This allows for high angle- and energy-dependent selectivity of the ionization channel. Altogether, this leads to excellent spin selectivity, as demonstrated below. Note that one can also select a specific ionization channel (for noble gases $J = 3/2$), by choosing a spectrally narrow photon energy below any of the higher-lying ionization channels [14–20].

The qualitative effect of the CM on the photoelectron spin identified by Fano is not unique to caesium, but the quantitative strength is. We find that in argon and xenon, the rare gas atoms that exhibit well-known Cooper minima, the associated spin polarization is only about 2%. Therefore, it is desirable to find an alternative path to generate spin-polarized photoelectrons from these targets. Indeed, we find substantially higher spin polarization in the vicinity of the Fano resonances, in excess of 40%. Furthermore, if measured in coincidence with the ion, angularly resolved photoelectron spectra show spin polarization approaching 100%. We complement our numerical calculations with a simple analytical model describing the

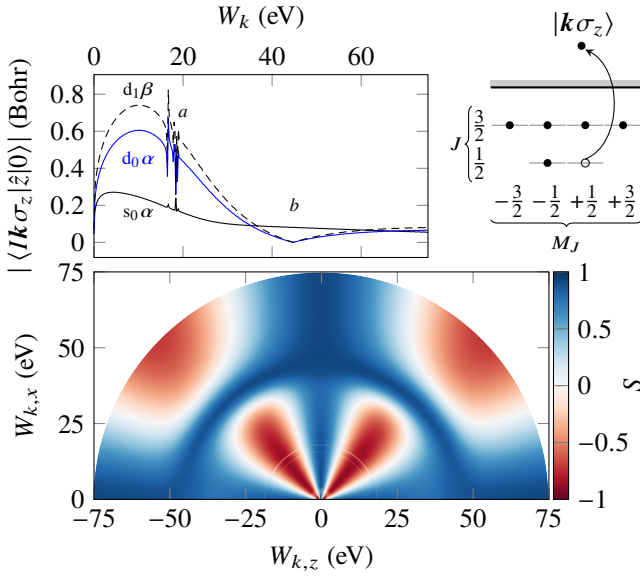


FIG. 1. Argon photoionization dipole matrix elements (*top left*) measured in coincidence with the ion in the $3p_{1/2}^{-1}$, $M_J = 1/2$ state (*top right*), for the LP dipole moment. The different lines correspond to contributions from different partial waves and spins (solid spin-up and dashed spin-down). The Fano resonances leading to the $3s_{1/2}^{-1}$ threshold are indicated by *a* and the location of the CM by *b*. Shown is also the resultant spin polarization (*bottom*), where in particular the CM manifests itself as a circle around $W_k = 50$ eV where the emitted photoelectron is 100 % spin-up.

underlying physical effect.

The spin polarization along the quantization axis $+z$, for one-photon ionization into a state with photoelectron momentum \mathbf{k} , is given by the photoionization matrix elements between the ground state and the final scattering state [1]:

$$S_z^I \stackrel{\text{def}}{=} \frac{P_{I\alpha} - P_{I\beta}}{P_{I\alpha} + P_{I\beta}} \approx \frac{|\langle I\mathbf{k}_\alpha | \hat{d} | 0 \rangle|^2 - |\langle I\mathbf{k}_\beta | \hat{d} | 0 \rangle|^2}{|\langle I\mathbf{k}_\alpha | \hat{d} | 0 \rangle|^2 + |\langle I\mathbf{k}_\beta | \hat{d} | 0 \rangle|^2}. \quad (1)$$

Here, $P_{I\alpha,\beta}$ are the probabilities of measuring an α (spin-up) or β (spin-down) electron, respectively, $|I\rangle$ denotes the final state of the ion (configuration $n\ell_J^{-1}$ and magnetic quantum number M_J), $|0\rangle$ the ground state of the atom. Finally, $\hat{d} = \hat{z}$ for linearly polarized (LP) light, $\hat{d} = (\hat{x} + i\xi\hat{y})/\sqrt{2}$ with $\xi = 1$ referred to as right-hand circularly polarized (RCP) light, and $\xi = -1$ referred to as left-hand circularly polarized (LCP) light. Summing over the final ion states, yields the total (overall) spin polarization:

$$S_z^{(\text{tot})} \approx \frac{\sum_I |\langle I\mathbf{k}_\alpha | \hat{d} | 0 \rangle|^2 - |\langle I\mathbf{k}_\beta | \hat{d} | 0 \rangle|^2}{\sum_I |\langle I\mathbf{k}_\alpha | \hat{d} | 0 \rangle|^2 + |\langle I\mathbf{k}_\beta | \hat{d} | 0 \rangle|^2}. \quad (2)$$

Conservation of angular momentum dictates that photoionization by LP light (which carries no spin-angular momentum) cannot generate net spin-angular momentum upon photoionization of a spin-0 target, such as the noble gas atoms initially in their ground state: $S_z^{(\text{tot})} = 0$. We note in passing, however, that

ion-channel resolved spin polarization may be non-zero even in this case [21], provided the photoelectron is measured in coincidence with the ion, including measuring the M_J quantum number, thereby establishing the chiral reference frame (the so-called ‘‘chiral observer’’ [22]). This is a formidable task. Another viewpoint is that for spin polarization to occur, we need to be able to trace the photoelectron back to the M_J it originated from, which for LP is only possible if the ion is simultaneously measured. For circular polarization, this selection of M_J happens naturally [5].

To compute the spin polarization, we thus need the dipole matrix elements from the ground state (or in general any bound state) to the scattering states, resolved on ion channel and photoelectron momentum and spin. These matrix elements are computed using the multi-channel extension of the infinite-time surface flux technique [23] described in [24]:

$$\langle I\mathbf{k}_{\sigma_z} | \hat{d} | 0 \rangle = \sqrt{N} \langle \mathbf{k}_{\sigma_z} | [\hat{h}_S, \theta(r_s)] | I | (\hat{H}_0 - \epsilon)^{-1} \hat{d} | 0 \rangle, \quad (3)$$

where \hat{h}_S is the asymptotic Hamiltonian obeyed by the wavefunction and the scattering state in the region beyond the matching surface r_s , $\epsilon = E_I + k^2/2$ is the total energy of the scattering state, and the resolvent $(\hat{H}_0 - \epsilon)^{-1}$, intimately related to inverse iterations, formally propagates the wavefunction from the time of the perturbation to the time of detection. The full derivation is given in [24].

The advantage of this expression, compared to the volume integral of the left-hand side of Eq. (3), is that we can compute the action of the resolvent on the dipole-disturbed ground state in linear time. The remaining surface integral reduces to linear combinations of the wavefunction amplitudes and derivatives at $r = r_s$ with the corresponding amplitudes and derivatives of the scattering states, since they are expanded in terms of spherical harmonics. The scattering states are accurately evaluated in terms of Coulomb waves [25]. The electronic structure is described in the Supplementary Information (SI) [26].

As an illustrative example, we show in Fig. 1 the dipole matrix elements for ionization using LP into the $3p_{1/2}^{-1}$, $M_J = 1/2$ channel of argon, calculated according to Eq. (3) (see the SI [26] for the very similar dipole moments for LCP and RCP). The Cooper minimum around $W_k = 45$ eV is clearly visible in that the matrix elements for ionization to the d symmetry vanishes there [27], leaving only the s contribution, which is spin pure. Precisely at the CM, we thus expect 100 % spin polarization of the photoelectron, when measured in coincidence with the photoion. This is indeed the case, as we see in Fig. 1, and this remains true if we angularly integrate the spin-resolved photoelectron distribution before computing the spin polarization; see Fig. 2. For an independent confirmation based on the solution of the Dirac equation, we compute the spin-resolved time-dependent ionization fluxes using the relativistic time-dependent configuration-interaction singles (RT-DCIS) [28, 29], for an ionizing pulse of finite duration (300 as $\Rightarrow \sim 6$ eV bandwidth; 1 TW/cm²) and a set of photon energies around the CM; see the SI [26] for a description on how the spin-resolved populations are extracted from the fluxes. We

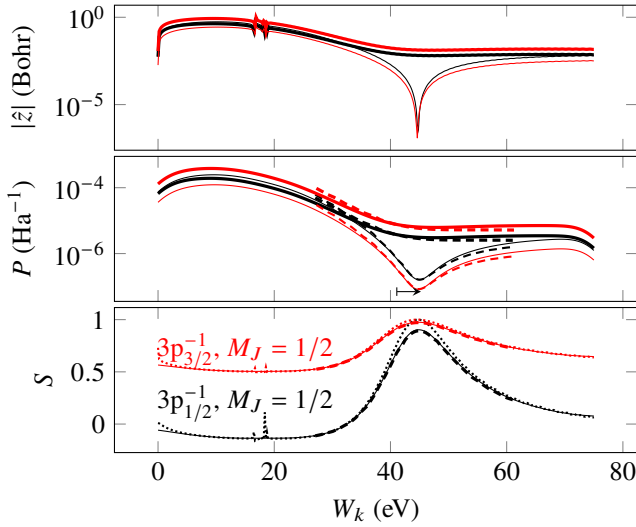


FIG. 2. Argon angle-integrated spin-resolved populations and spin polarization when measured in coincidence with the ion in the $3p_{1/2}^{-1}, M_J = 1/2$ state (black lines) or in the $3p_{3/2}^{-1}, M_J = 1/2$ state (red lines), for LP. *Top panel*: squared dipole matrix elements computed using the PT Eq. (3), thick lines α , thin lines β); *middle panel*: solid lines spin-resolved populations after convolving the dipole matrix elements with a Gaussian spectrum of 6 eV bandwidth, dashed lines using time-propagation of the RTDCIS (see main text); *bottom panel*: spin polarization, dotted lines computed using the PT results from the top panel, solid lines convolved PT results, dashed lines using RTDCIS. The RTDCIS results have been blueshifted by 4.25 eV to align the CM between the calculations.

find the predicted spin polarizations to be in good agreement, when considering that convolving with the finite pulse smooths out the infinite-time response computed by perturbation theory and Eq. (1).

Once we average over all ionic states, the spin polarization is substantially reduced, reaching a meagre 2% in the vicinity of the Cooper minimum, see Fig. 3. This is in contrast to the case of caesium [1, 6], where around 85% spin polarization was demonstrated, even when angularly integrating the photoelectron distribution. Naturally, overall spin polarization is absent for LP. For the Fano resonances, the spin polarization remains high (reaching up to 40%).

What makes the CM of argon (and xenon) different from that of caesium, and why are the Fano resonances an efficient source of spin polarization? For argon (and xenon), where we ionize from $np^6 \ ^1S_0$ into $np^5 \ (^2P^o) \ k\ell, J = 3/2, 1/2, \ell = s, d$, we have the following contributions:

$$P_{J\sigma_z} = |A_{J\sigma_z}|^2 \stackrel{\text{def}}{=} |\langle k\ell'_{\sigma_z} m'_{\ell'} | \mp r \hat{C}_{\pm 1}^{(1)} | np_J m_J \rangle|^2, \quad (4)$$

where the upper (lower) sign corresponds to RCP (LCP). Evaluating the spin-angular integrals (see the SI [26]), summing over $\ell', m'_{\ell'}$, and m_J , and denoting the radial integrals as $R_{\ell', J}$,

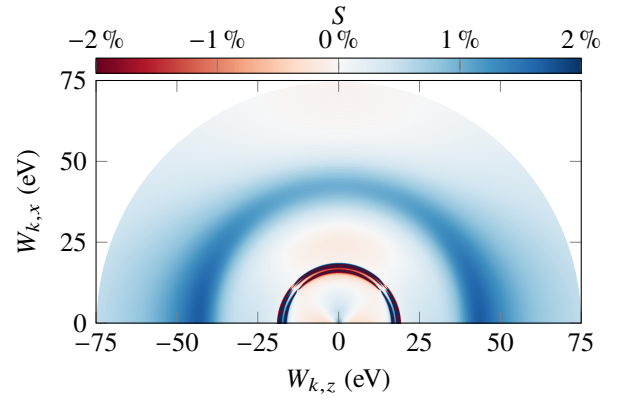


FIG. 3. Angle-resolved argon total spin polarization, i.e. obtained by summing over all ion channels, when ionizing with LCP light (RCP will give exactly the opposite result, and LP will yield exactly zero spin polarization). Note that the colour scale saturates at $\pm 2\%$, which is the approximate maximum spin polarization obtained in the vicinity of the CM, whereas in the region of the Fano resonances, the spin polarization exceeds 40%.

we find

$$\begin{bmatrix} P_{3/2\alpha} \\ P_{3/2\beta} \\ P_{1/2\alpha} \\ P_{1/2\beta} \end{bmatrix} = C_{\text{pol}} \begin{bmatrix} |R_{s,3/2}|^2 \\ |R_{d,3/2}|^2 \\ |R_{s,1/2}|^2 \\ |R_{d,1/2}|^2 \end{bmatrix}, \quad (5)$$

$$C_{\text{RCP}} = \frac{1}{9} \begin{bmatrix} 1 & 5 & 0 & 0 \\ 3 & 3 & 0 & 0 \\ 0 & 0 & 2 & 1 \\ 0 & 0 & 0 & 3 \end{bmatrix}, \quad C_{\text{LCP}} = \frac{1}{9} \begin{bmatrix} 3 & 3 & 0 & 0 \\ 1 & 5 & 0 & 0 \\ 0 & 0 & 0 & 3 \\ 0 & 0 & 2 & 1 \end{bmatrix}, \quad (6)$$

where the upper-left quadrant pertains to the $J = 3/2$ channel, and the lower-right to the $J = 1/2$ channel. From this, we see that for a $J = 1/2$ ion, we expect 100% spin-up (spin-down) photoelectron for RCP (LCP) at the CM, where the radial integral $R_{d,1/2}$ vanishes:

$$S = \pm \frac{2-0}{2+0} = \pm 1. \quad (7)$$

For a $J = 3/2$ ion, again at the CM where this time $R_{d,3/2}$ vanishes, we only expect partial spin polarization:

$$S = \pm \frac{1-3}{1+3} = \mp \frac{1}{2}, \quad (8)$$

consistent with the results observed in Fig. 4. If we instead do not observe the ion, again assuming that $R_{d,J}$ vanish, we expect the spin polarization to be

$$S = \pm \frac{1+2-3}{1+2+3} = 0. \quad (9)$$

The reason why we observe any spin polarization at all is because the Cooper minima for $J = 1/2$ and $J = 3/2$ are not

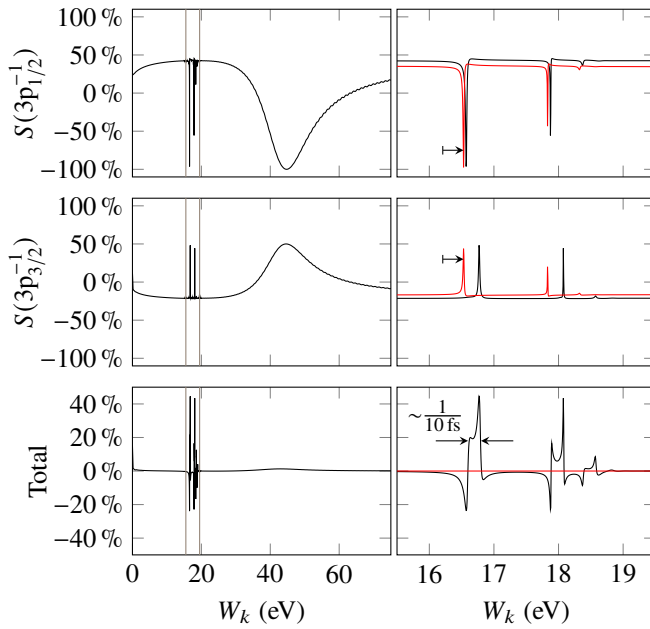


FIG. 4. Argon angle-integrated photoelectron spin polarization for LCP light, resolved on ion energy level, i.e. which hole and J , but not M_J , as well as total. The *left column* shows the entire energy range, including the CM. The *right column* focuses on the Fano resonances leading up to the the $3s_{1/2}^{-1}$ threshold, in the energy range delimited by the vertical lines in the left column. The black lines result from a calculation with ECP (i.e. quasirelativistic, including spin-orbit coupling). It is clearly visible that the Fano lines for $J = 1/2$ are shifted with respect to those for $J = 3/2$, a necessary condition for the generation of total spin polarization. The red lines, on the other hand, are the result of an all-electron, non-relativistic calculation; these have been blue-shifted by 0.33 eV (as indicated by the arrow) to align the $3s_{1/2}^{-1}$ threshold with the ECP calculation. In this case, the Fano lines for $J = 1/2$ and $J = 3/2$ appear at exactly the same energies, and therefore the spin polarization perfectly cancels when summing over all ion channels.

perfectly aligned, i.e. $R_{d,1/2}$ and $R_{d,3/2}$ do not vanish simultaneously. Additionally, $R_{s,1/2}$ and $R_{s,3/2}$ may differ slightly.

However, the presence of Fano resonances in argon with very rapid variation of the dipole matrix elements [30–33] more than makes up for this deficiency; the spectral feature around 16.7 eV in Fig. 4 is approximately 0.2 eV wide. This implies that ionizing with an LCP pulse centred at 16.7 eV that is about 10 fs long, will yield photoelectrons with spin polarization in excess of 20 %, even when *integrating over all angles and not measuring the ion*; using a longer pulse results in spin polarization up to 40 %.

We may perform the same analysis for xenon. There the situation is more complex, due to the higher number of channels and the giant dipole resonance present at around $W_k = 100$ eV, which leads to additional structures in the dipole matrix elements, illustrated for the $5p_{1/2}^{-1}$, $M_J = -1/2$ in Fig. 5. Again, we predict perfect spin polarization in the vicinity of the two CM (around 50 eV and 200 eV, respectively), this time 100 % *spin-down*, since we consider the $M_J = -1/2$ channel, i.e. the

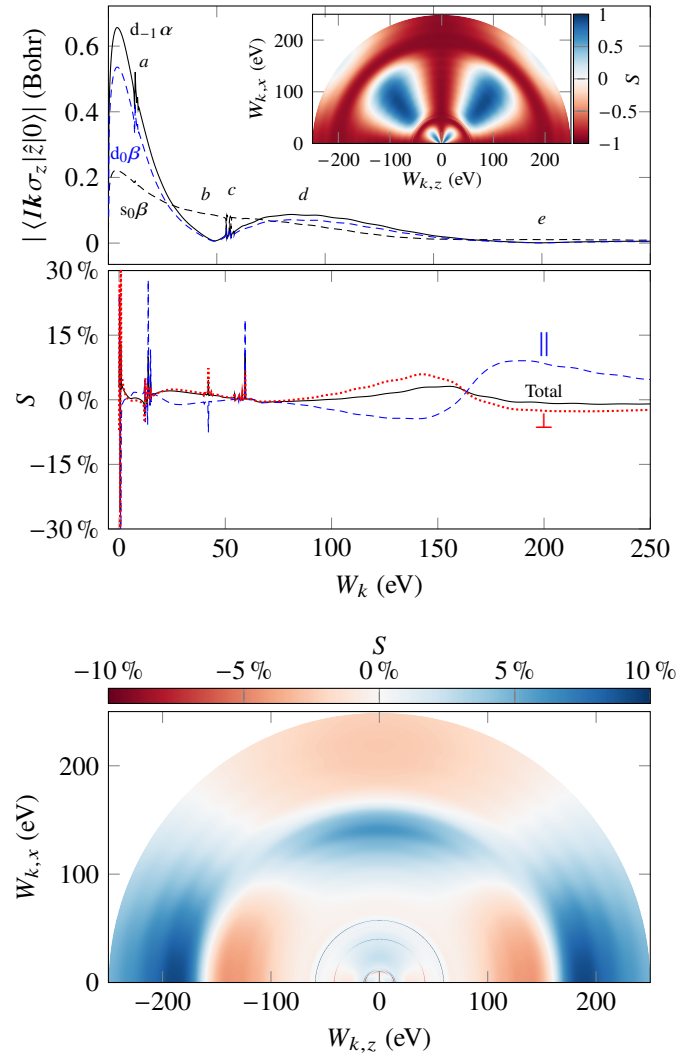


FIG. 5. *Top panel*: Xenon photoionization dipole matrix elements in the ionization channel $5p_{1/2}^{-1}$, $M_J = -1/2$, for the dipole moment along the z axis (see the SI [26] for the very similar dipole moments for LCP and RCP). The different lines correspond to contributions from different partial waves and spins (solid spin-up and dashed spin-down). We observe two sets of Fano resonances, the first (indicated by a) are due to the Rydberg states leading up to the $5s_{1/2}^{-1}$ threshold at around $W_k = 16$ eV, and similarly, the second (c) are due to the $4d_{5/2}^{-1}$ threshold at around 59 eV. Additionally, the correlation-induced [34] CM (b) around 50 eV, the giant dipole resonance (d) around 100 eV, and a CM-like feature (e) around 200 eV are clearly visible. *Middle panel*: Xenon total spin polarization, i.e. obtained by summing over all ion channels, when ionizing with LCP light (RCP will give exactly the opposite result, and LP will yield exactly zero spin polarization), in the vicinity of the Fano resonances, the Cooper minimum, and the giant dipole resonance. The solid black line corresponds to angle-integrated spin-polarization; the dashed blue corresponds to emission along the forward direction (the backward direction is by symmetry exactly the same); the dotted red line corresponds to emission perpendicular to the polarization direction. *Bottom panel*: Total spin polarization from xenon, resolved on the emission angle.

“mirror case” of $M_J = 1/2$. Again, when considering the total spin polarization (see Fig. 5), i.e. when averaging over the ionic states, the spin polarization is rather small in the vicinity of the CM and the giant dipole resonance, due the presence of many more channels than in caesium. Again, the spin polarization is rather sizeable in the vicinity of the Fano resonances (of which there are more than in argon), exceeding 30 %, for some energies. In contrast to argon, the total spin polarization depends strongly on the photoelectron emission angle, with opposite sign along and perpendicular to the polarization direction.

The work of SC has been supported through scholarship 185-608 from *Olle Engkvists Stiftelse*. JMD acknowledges support from the *Knut and Alice Wallenberg Foundation* (2017.0104 and 2019.0154), the Swedish Research Council (2018-03845) and *Olle Engkvists Stiftelse* (194-0734). MI acknowledges support from *FET-OPEN “OPTologic”* (899794). OS acknowledges support from *Horizon Europe* ERC-2021-ADG (101054696 *Ulisses*).

-
- [1] U. Fano, *Physical Review* **178**, 131 (1969).
- [2] Z. Nie, F. Li, F. Morales, S. Patchkovskii, O. Smirnova, W. An, N. Nambu, D. Matteo, K. A. Marsh, F. Tsung, W. B. Mori, and C. Joshi, *Physical Review Letters* **126**, 054801 (2021).
- [3] Z. Nie, F. Li, F. Morales, S. Patchkovskii, O. Smirnova, W. An, C. Zhang, Y. Wu, N. Nambu, D. Matteo, K. A. Marsh, F. Tsung, W. B. Mori, and C. Joshi, *Physical Review Research* **4**, 033015 (2022).
- [4] M. Ruberti, V. Averbukh, and F. Mintert, *Physical Review X* **14**, 041042 (2024).
- [5] I. Barth and O. Smirnova, *Physical Review A* **88**, 013401 (2013).
- [6] U. Heinzmann, J. Kessler, and J. Lorenz, *Physical Review Letters* **25**, 1325 (1970).
- [7] P. Lambropoulos, *Physical Review Letters* **30**, 413 (1973).
- [8] G. L. Yudin and M. Y. Ivanov, *Physical Review A* **64**, 10.1103/physreva.64.013409 (2001).
- [9] I. Barth and O. Smirnova, *Journal of Physics B: Atomic, Molecular and Optical Physics* **47**, 204020 (2014).
- [10] I. Barth and M. Lein, *Journal of Physics B: Atomic, Molecular and Optical Physics* **47**, 204016 (2014).
- [11] A. Hartung, F. Morales, M. Kunitski, K. Henrichs, A. Laucke, M. Richter, T. Jahnke, A. Kalinin, M. Schöffler, L. P. H. Schmidt, M. Ivanov, O. Smirnova, and R. Dörner, *Nature Photonics* **10**, 526 (2016).
- [12] D. Trabert, A. Hartung, S. Eckart, F. Trinter, A. Kalinin, M. Schöffler, L. P. H. Schmidt, T. Jahnke, M. Kunitski, and R. Dörner, *Physical Review Letters* **120**, 043202 (2018).
- [13] S. Svensson, N. Mårtensson, E. Basilier, P. A. Malmquist, U. Gelius, and K. Siegbahn, *Physica Scripta* **14**, 141 (1976).
- [14] D. Dill, *Physical Review A* **7**, 1976 (1973).
- [15] C. M. Lee, *Physical Review A* **10**, 1598 (1974).
- [16] U. Fano, *Journal of the Optical Society of America* **65**, 979 (1975).
- [17] J. Geiger, *Zeitschrift für Physik A: Atoms and Nuclei* **282**, 129 (1977).
- [18] W. R. Johnson, K. T. Cheng, K.-N. Huang, and M. L. Dourneuf, *Physical Review A* **22**, 989 (1980).
- [19] U. Heinzmann, *Journal of Physics B: Atomic and Molecular Physics* **13**, 4353 (1980).
- [20] U. Heinzmann, *Journal of Physics B: Atomic and Molecular Physics* **13**, 4367 (1980).
- [21] S. Carlström, J. M. Dahlström, M. Y. Ivanov, O. Smirnova, and S. Patchkovskii, *Physical Review A* **108**, 043104.
- [22] D. Ayuso, A. F. Ordonez, and O. Smirnova, *Physical Chemistry Chemical Physics* **24**, 26962 (2022).
- [23] F. Morales, T. Bredtmann, and S. Patchkovskii, *Journal of Physics B: Atomic, Molecular and Optical Physics* **49**, 245001 (2016).
- [24] S. Carlström, M. Spanner, and S. Patchkovskii, *Physical Review A* **106**, 043104 (2022).
- [25] A. R. Barnett, The calculation of spherical Bessel and Coulomb functions, in *Computational Atomic Physics*, Computational Atomic Physics (Springer Berlin Heidelberg, 1996) pp. 181–202.
- [26] See Supplementary Information at [URL will be inserted by publisher].
- [27] J. W. Cooper, *Physical Review* **128**, 681 (1962).
- [28] F. Zapata, J. Vinbladh, A. Ljungdahl, E. Lindroth, and J. M. Dahlström, *Physical Review A* **105**, 012802 (2022).
- [29] R. Tahouri, A. Papoulia, S. Carlström, F. Zapata, and J. M. Dahlström, *Communications Physics* **7**, 344 (2024).
- [30] A. F. Starace, *Physical Review A* **16**, 231 (1977).
- [31] P. van der Meulen, M. O. Krause, and C. A. de Lange, *Physical Review A* **43**, 5997 (1991).
- [32] S. Sorensen, T. Åberg, J. Tulkki, E. Rachlew-Källne, G. Sundström, and M. Kirm, *Physical Review A* **50**, 1218 (1994).
- [33] T. Carette, J. M. Dahlström, L. Argenti, and E. Lindroth, *Physical Review A* **87**, 10.1103/physreva.87.023420 (2013).
- [34] M. Kutzner, V. Radojević, and H. P. Kelly, *Physical Review A* **40**, 5052 (1989).
- [35] D. A. Varshalovich, *Quantum Theory of Angular Momentum: Irreducible Tensors, Spherical Harmonics, Vector Coupling Coefficients, 3nj Symbols* (World Scientific Pub, Singapore Teaneck, NJ, USA, 1988).
- [36] A. Nicklass, M. Dolg, H. Stoll, and H. Preuss, *The Journal of Chemical Physics* **102**, 8942 (1995).
- [37] K. A. Peterson, D. Figgen, E. Goll, H. Stoll, and M. Dolg, *The Journal of Chemical Physics* **119**, 11113 (2003)

SUPPLEMENTARY INFORMATION

Electronic structure

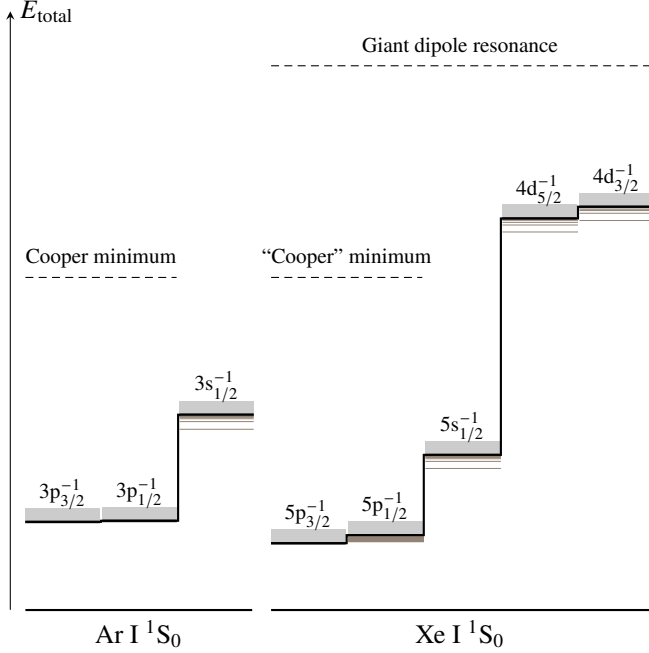


FIG. SI–1. Sketch of the energy structures of argon and xenon; the dashed line indicates the position of the CM in the $3p_{3/2}^{-1}$ and $3p_{1/2}^{-1}$ channels in argon. Also in xenon, there is a minimum in the matrix elements just before the giant resonance, which is similar to a CM, but is correlation-induced due to the interaction with the 4d electrons [34]. The sketch is to scale with energies as listed in Table I. Also shown are the autoionizing states in each channel that will lead to Fano resonances in all channels shown to the left of them (i.e. with lower I_p).

The ground state $|0\rangle$ is approximated using the Hartree–Fock solution. Since we wish to consider the spin–orbit interaction, the orbitals are expanded in two-component spinor spherical harmonics (see section 7.2 of [35]) which are eigenfunctions of \hat{L}^2 , \hat{S}^2 , \hat{J}^2 , and \hat{J}_z . The spin–orbit interaction is thus diagonal in this basis, and is implemented using effective core potentials (ECPs), which account for scalar- and vector-relativistic effects. For argon, we use the large-core ECP by Nicklass *et al.* [36], and for xenon the small-core ECP by Peterson *et al.* [37]. The ion states $|I\rangle$ are approximated at the configuration-interaction singles (CIS) level, which corresponds to removal of one electron, with the remaining orbitals frozen, i.e. no relaxation. This leads to slightly too high ionization potentials, especially for inner electrons, as seen in Table I. In the calculations presented in this work, ionization was only permitted from 3s–3p in case of argon, and from 4d–5p in case of xenon (see Fig. SI–1).

TABLE I. Theoretical ionization potentials of the ns and np electrons of argon and xenon, compared with their experimental and relativistic theoretical values (Refs: [SI1]^a, [SI2]^b, [SI3]^c, [SI4]^d, [SI5]^e, [SI6]^f, [SI7]^g, [28]^h).

Element	Hole	I_p (eV)	Exp. (eV)	Δ (eV)	Rel. Δ (%)	I_p (eV)
Ar	$3p_{3/2}^{-1}$	15.871	15.760 ^a	0.111	0.7	15.995 ^h
	$3p_{1/2}^{-1}$	16.069	15.937 ^b	0.132	0.8	16.201 ^h
	$3s_{1/2}^{-1}$	35.159	29.239 ^b	5.920	20.2	35.010 ^h
Xe	$5p_{3/2}^{-1}$	12.026	12.130 ^c	−0.104	−0.9	11.965 ^h
	$5p_{1/2}^{-1}$	13.483	13.436 ^d	0.047	0.3	13.407 ^h
	$5s_{1/2}^{-1}$	27.927	23.397 ^d	4.530	19.4	27.507 ^h
	$4d_{5/2}^{-1}$	70.481	67.55 ^e	2.98	4.4	71.640 ^h
	$4d_{3/2}^{-1}$	72.591	69.52 ^e	3.09	4.4	73.760 ^h
	$4p_{3/2}^{-1}$	162.450	145.5 ^f	16.950	11.6	162.801 ^h
	$4p_{1/2}^{-1}$	175.522	146.7 ^g	28.822	19.6	175.610 ^h
	$4s_{1/2}^{-1}$	228.995	213.2 ^f	15.795	7.4	229.474 ^h

Dipole matrix elements

The dipole moments \hat{x} , \hat{y} , and \hat{z} can be written in terms of the components of the spherical tensor $\hat{C}^{(1)}$ as

$$\hat{x} = \frac{r}{\sqrt{2}}[-\hat{C}_1^{(1)} + \hat{C}_{-1}^{(1)}], \quad \hat{y} = \frac{r}{\sqrt{2}}[i\hat{C}_1^{(1)} + i\hat{C}_{-1}^{(1)}], \quad \hat{z} = r\hat{C}_0^{(1)}. \quad (\text{SI-1})$$

\hat{x} and \hat{y} thus have precisely the same angular structure, i.e. they both couple to $m'_\ell = m_\ell \pm 1$, but with different complex phases. The difference in phase between the matrix element of \hat{x} and \hat{y} is what leads to the asymmetry in spin polarization between LCP [$(\hat{x} - i\hat{y})/\sqrt{2} \equiv r\hat{C}_{-1}^{(1)}$] and RCP [$(\hat{x} + i\hat{y})/\sqrt{2} \equiv -r\hat{C}_1^{(1)}$]; see Fig. SI–2 for argon and Fig. SI–3 for xenon. Additionally, J -resolved (i.e. traced over M_J) spin polarizations are shown in Fig. SI–4 and Fig. SI–5 for argon and xenon, respectively.

The explicit formula for the ion- and electron-spin-resolved dipole matrix elements from the ground state $np^6 \ ^1S_0$ is given by

$$\begin{aligned} A_{J\sigma_z} &= \langle k\ell'_{\sigma_z} m'_\ell | \mp r \hat{C}_{\pm 1}^{(1)} | np_J m_J \rangle \\ &= \mp R_{\ell', J} \langle \ell' m'_\ell | \hat{C}_{\pm 1}^{(1)} | p m_\ell \rangle C_{p, m_\ell; \frac{1}{2}, \sigma_z}^{J, m_J} \\ &= \mp [2\ell' + 1]^{-1} R_{\ell', J} C_{p, m_\ell; 1, \pm 1}^{\ell', m'_\ell} \langle \ell' | \hat{C}_{\pm 1}^{(1)} | p \rangle C_{p, m_\ell; \frac{1}{2}, \sigma_z}^{J, m_J} \\ &= \mp \sqrt{3} [2\ell' + 1]^{-1} R_{\ell', J} C_{p, m_\ell; 1, \pm 1}^{\ell', m'_\ell} C_{p, 0; 1, 0}^{\ell', 0} C_{p, m_\ell; \frac{1}{2}, \sigma_z}^{J, m_J}, \end{aligned} \quad (\text{SI-2})$$

where

$$R_{\ell', J} \stackrel{\text{def}}{=} \int_0^\infty dr P(k\ell'; r) r P(np_J; r). \quad (\text{SI-3})$$

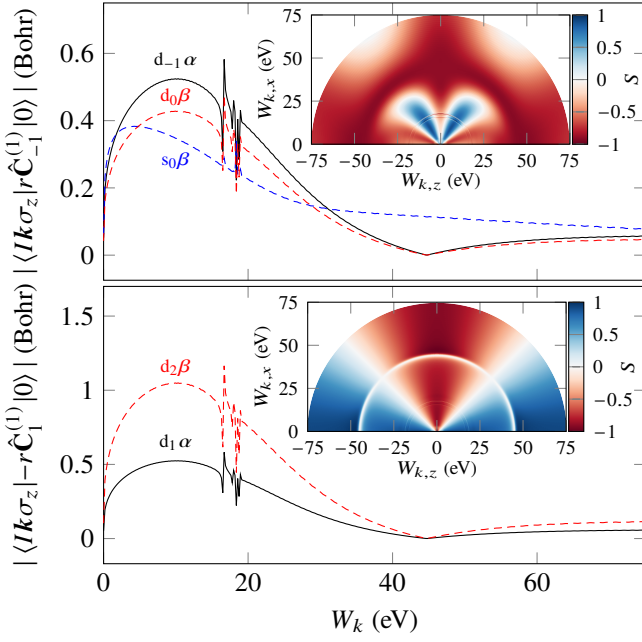


FIG. SI-2. Argon photoionization dipole matrix elements in the ionization channel $3p_{1/2}^{-1}$, $M_J = 1/2$, for the dipole moments for LCP (*top panel*), and RCP (*bottom panel*). These are formed from linear combinations of \hat{x} and \hat{y} (see main text). The different lines correspond to contributions from different partial waves and spins (solid spin-up and dashed spin-down).

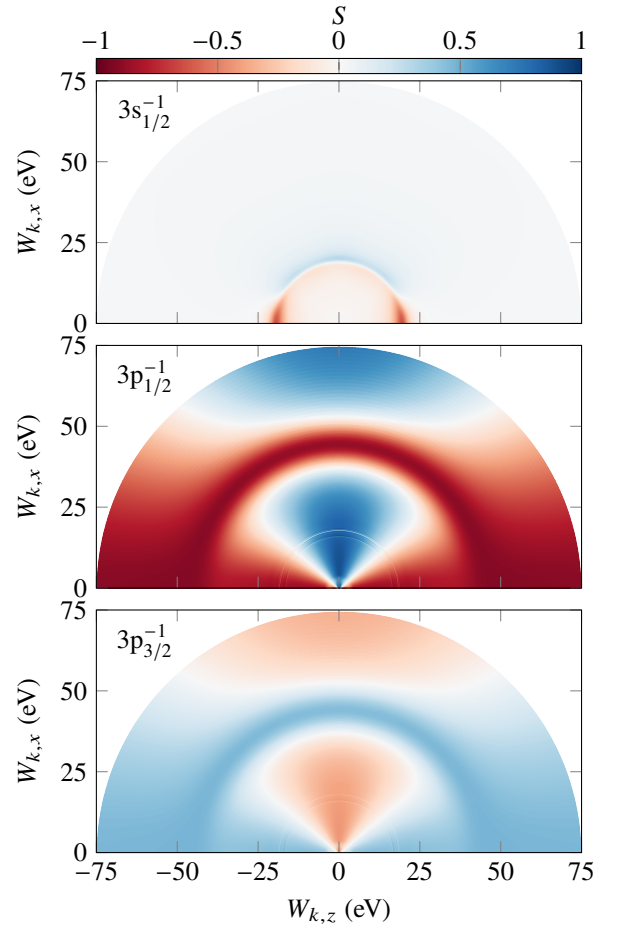


FIG. SI-4. Ion-resolved (i.e. J -resolved) spin polarization for LCP ionization (RCP will give exactly the opposite result, and LP will yield exactly zero spin polarization) of argon.

Technical details on computing spin polarization

Computing the spin polarization according to Eq. (1) of the main article, care is needed when P_α and P_β vanish simultaneously. Otherwise, due to numerical round-off errors, one might divide something small by zero, and the computed spin polarization will then exhibit spikes. One way of circumventing this is to add a regulator to the denominator, or better a small fraction of a smoothed copy of the denominator itself:

$$S \stackrel{\text{def}}{=} \frac{P_\alpha - P_\beta}{\Xi(P_\alpha + P_\beta)}, \quad \Xi(y) = y + \epsilon \langle y \rangle, \quad (\text{SI-4})$$

where $\langle y \rangle$ is a smooth version of y , and ϵ a scaling factor.

When the electron is measured in coincidence with the ion, resolved on J and M_J , the coordinate system of the ion is *fully* specified, i.e. not only the quantization axis z , which is set by the external field, but also x and y . Since these are typically not fixed in the experiment, they must be averaged over; it is not enough to sum over M_J . If this is not done, a preferred orientation of the universe is chosen, and spin

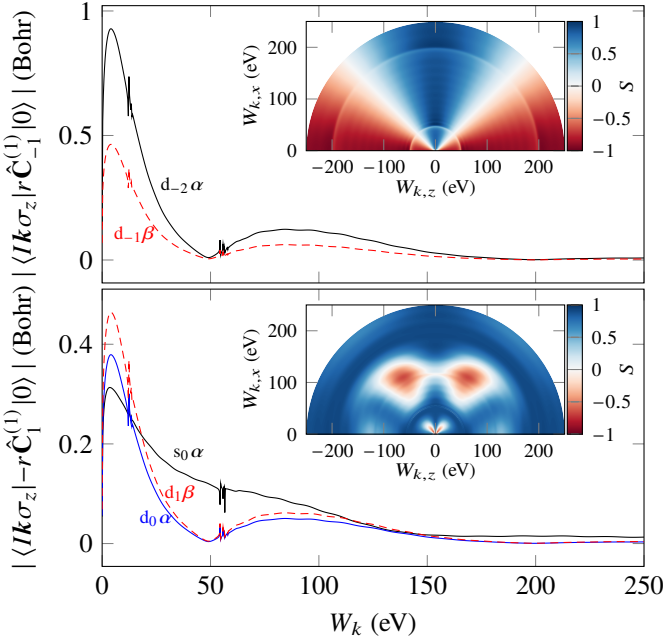


FIG. SI-3. Xenon photoionization dipole matrix elements in the ionization channel $5p_{1/2}^{-1}$, $M_J = -1/2$, for the dipole moments for LCP (*top panel*), and RCP (*bottom panel*). The different lines correspond to contributions from different partial waves and spins (solid spin-up and dashed spin-down).

polarization dependent on the photoelectron emission angle ϕ will be observed.

Description of RTDCIS calculations

The electronic structure described above is only quasirelativistic, and we use the RTDCIS [28, 29] calculations as an independent, fully-relativistic benchmark of our perturbation theory results. These calculations are however limited to LP at the moment. They provide the particle-hole channel-resolved photoelectron populations characterized by the quantum numbers ℓ , j , and m_j . Given a relativistic hole a in the ion, we define a one-electron time-dependent orbital as: $|\chi_a(t)\rangle = \sum_p c_a^p(t) |\phi_p\rangle$ where $|\phi_p\rangle$ are virtual electron orbitals with energies ϵ_p , and $c_a^p(t)$ are their time-dependent complex amplitudes [SI8]. For a given particle-hole channel, the final photoelectron population is given by $P_a^{\ell j m_j} = \lim_{t \rightarrow \infty} \sum_p |c_a^p(t)|^2$. We obtain the absolute value of the resonant complex amplitude as $|c_a^{\ell j m_j}| = (P_a^{\ell j m_j})^{1/2}$ with $\epsilon_p \approx \epsilon_a + \omega$, where the $P_a^{\ell j m_j}$ is computed using RTDCIS, and ϵ_a is the energy of the occupied orbital $|\phi_a\rangle$.

The ℓ -, m_ℓ - and spin-resolved probabilities associated with a given hole a are given by:

$$P_a^{\ell m_\ell m_s} = \lim_{t \rightarrow \infty} \langle \chi_a(t) | \ell m_\ell m_s \rangle \langle \ell m_\ell m_s | \chi_a(t) \rangle,$$

$$c_a^{\ell m_\ell m_s}(t) \stackrel{\text{def}}{=} \langle \ell m_\ell m_s | \chi_a(t) \rangle = \langle \ell m_\ell m_s | \ell j m_j \rangle \langle \ell j m_j | \chi_a(t) \rangle$$

$$= \langle \ell m_\ell m_s | \ell j m_j \rangle c_a^{\ell j m_j}(t),$$

(SI-5)

where we implicitly sum over j and m_j . If there is only one j involved, the spin probabilities $P_a^{\ell m_\ell m_s}$ can be expressed as a function of the absolute values of the complex amplitudes, $|c_a^{\ell j m_j}|$. When there are contributions from two states with same ℓ but different total angular momenta, $j_1 \neq j_2$, there are also cross terms involving the phase difference between the two complex amplitudes. This phase difference can be obtained by the ratio $\phi = \arg\{c_a^{\ell j_1 m_j} / c_a^{\ell j_2 m_j}\}$ [SI9]. According to perturbation theory, for LP these complex amplitudes are proportional to the matrix elements of the dipole operator \hat{z} : $c_a^{\ell j m_j} \propto \langle \epsilon_p \ell j m_j | \hat{z} | n' \ell' j' m_j \rangle$, where $|n' \ell' j' m_j\rangle$ and $|\epsilon_p \ell j m_j\rangle$ represent the hole and particle states, respectively. The complex amplitudes can be estimated with the aid of the Wigner-Eckart theorem:

$$c_a^{\ell j m_j} \propto \langle \epsilon_p \ell j m_j | \hat{z} | n' \ell' j' m_j \rangle$$

$$= (-)^{j-m_j} \begin{pmatrix} j & 1 & j' \\ -m_j & 0 & m_j \end{pmatrix} \langle \epsilon_p \ell j | r | n' \ell' j' \rangle \langle j || \hat{C}^{(1)} || j' \rangle$$

(SI-6)

where the reduced matrix element of the spherical tensors of rank k for half-integer angular momenta is given by [SI10]

$$\langle j || \hat{C}^{(k)} || j' \rangle = (-)^{j+1/2} [(2j+1)(2j'+1)]^{1/2} \begin{pmatrix} j & k & j' \\ 1/2 & 0 & -1/2 \end{pmatrix}.$$

(SI-7)

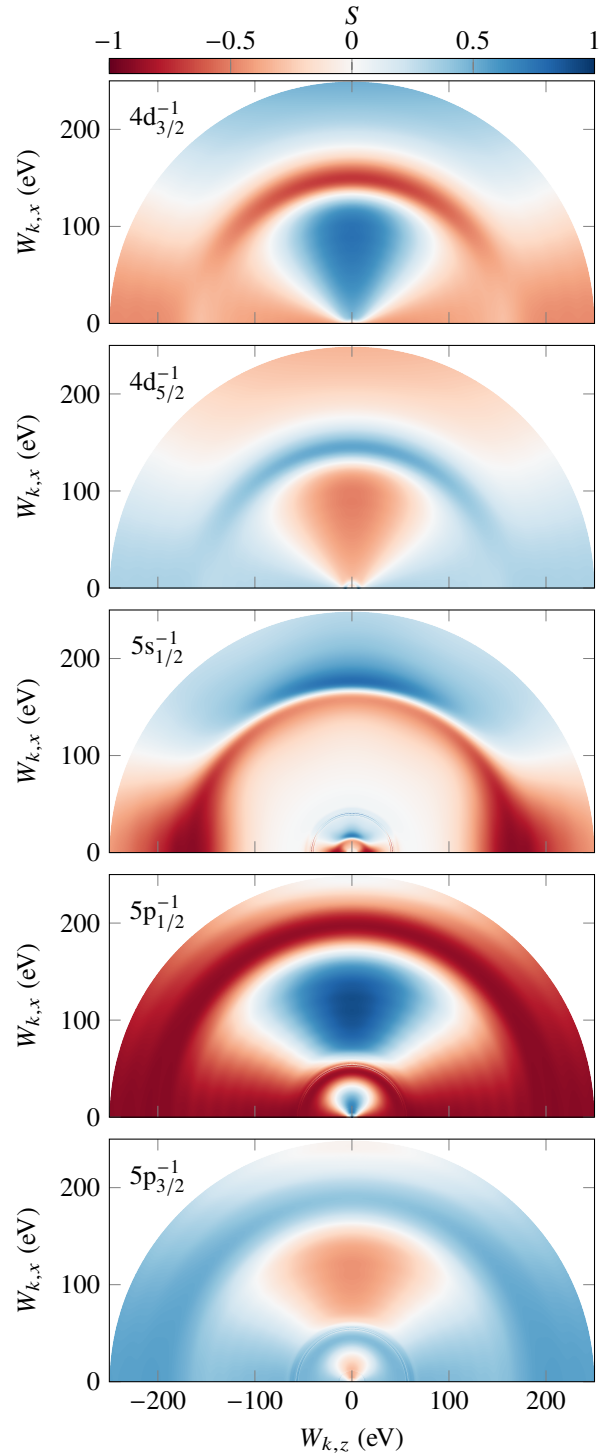


FIG. SI-5. Ion-resolved (i.e. J -resolved) spin polarization for LCP ionization (RCP will give exactly the opposite result, and LP will yield exactly zero spin polarization) of xenon.

-
- [SI1] I. Velchev, W. Hogervorst, and W. Ubachs, *Journal of Physics B: Atomic, Molecular and Optical Physics* **32**, L511 (1999).
- [SI2] E. B. Saloman, *Journal of Physical and Chemical Reference Data* **39**, 033101 (2010).
- [SI3] E. B. Saloman, *Journal of Physical and Chemical Reference Data* **33**, 765 (2004).
- [SI4] J. E. Hansen and W. Persson, *Phys. Scr.* **36**, 602 (1987).
- [SI5] K. Codling and R. P. Madden, *Physical Review Letters* **12**, 106 (1964).
- [SI6] *Photoemission in Solids I*, Topics in Applied Physics (Springer Berlin Heidelberg, 1978) pp. 265–274.
- [SI7] J. A. Bearden and A. F. Burr, *Reviews of Modern Physics* **39**, 125 (1967).
- [SI8] N. Rohringer, A. Gordon, and R. Santra, *Physical Review A* **74**, 043420 (2006).
- [SI9] J. M. Dahlström, S. Pabst, and E. Lindroth, *APL Photonics* **4**, 011101 (2019).
- [SI10] I. P. Grant, *Relativistic quantum theory of atoms and molecules: Theory and computation* (Springer, New York, 2007)